Open access • Journal Article • DOI:10.1617/S11527-011-9717-X

Monitoring the early-age hydration of self-compacting concrete using ultrasonic p-wave transmission and isothermal calorimetry — Source link

Bram Desmet, Kelly Chrysanthe Atitung, Miguel Angel Abril Sanchez, John Vantomme ...+9 more authors

Institutions: Royal Military Academy, Ghent University, Hogeschool Gent, Katholieke Universiteit Leuven

Published on: 25 Mar 2011 - Materials and Structures (Springer Netherlands)

Topics: Superplasticizer and Ultrasonic testing

Materials and Structures (2011) 44:1537–1558
DOI 10.1617/s11527-011-9717-x

ORIGINAL ARTICLE

Monitoring the early-age hydration of self-compacting concrete using ultrasonic p-wave transmission and isothermal calorimetry

Bram Desmet · Kelly Chrysanthe Atitung · Miguel Angel Abril Sanchez · John Vantomme · Dimitri Feys · Nicolas Robeyst · Katrien Audenaert · Geert De Schutter · Veerle Boel · Gert Heirman · Özlem Cizer · Lucie Vandewalle · Dionys Van Gemert

Received: 6 February 2010 / Accepted: 23 February 2011 / Published online: 25 March 2011

Abstract The early-age hydration (≤48 h) of a series of self-compacting concretes and corresponding mortars and one traditionally vibrated concrete and mortar is monitored in a continuous way using ultrasonic testing and isothermal calorimetry. The mixtures differ in type of mineral addition, superplasticizer, cement, cement-to-powder ratio and water-to-powder ratio. The influence of these different mixture compositions on the kinetics of the hydration during the first days of the hydration is characterized by the heat production rate q and the evolution of the p-wave velocity, which is a consequence of the microstructural changes. The variations in the acceleration caused by mineral additions and the deceleration caused by superplasticizers lead to a significantly different behavior. Separating the impact of each of the affecting factors is not always possible due to their combined actions. The nature of the acceleration due to limestone additions and the deceleration caused by polycarboxylate ether superplasticizers can be distinguished clearly, but cannot be quantified. The correlation between the ultrasonic and isothermal calorimetric results is investigated based on parameters related to the start and the end of the setting and reveals the meaningfulness of these parameters when assessing the hydration of self-compacting mixtures with continuous ultrasonic techniques.

Keywords Self-compacting concrete · Continuous ultrasonic testing · p-Wave hydration · Addition · Superplasticizer · Isothermal calorimetry

B. Desmet (✉) · K. C. Atitung · M. A. Abril Sanchez · J. Vantomme
Department of Civil and Materials Engineering, Royal Military Academy, Renaissancelaan 30, 1000 Brussels, Belgium
e-mail: bram.desmet@rma.ac.be

D. Feys · N. Robeyst · K. Audenaert · G. De Schutter
Magnel Laboratory for Concrete Research, Department of Structural Engineering, Faculty of Engineering Ghent University, Technologiepark-Zwijnaarde 904, 9052 Ghent, Belgium

V. Boel
Department of Construction, Faculty of Applied Engineering Sciences, University College Ghent, Schoonmeersstraat 52, 9000 Ghent, Belgium

G. Heirman · Ö. Cizer · L. Vandewalle · D. Van Gemert
Reyntjens Laboratory, Department of Civil Engineering, K.U.Leuven, Kasteelpark Arenberg 40, 3001 Heverlee, Belgium

1 Introduction

The self-compacting properties of SCC can be obtained in various ways, combining different kinds of mineral additions and/or viscosity modifying agents and superplasticizers (SP) and by carefully choosing the mixture design [1, 2]. Apart from the effects of the mixture design on the required self-compactibility, the different ingredients each also

have a very specific influence on the hydration mechanisms in the fresh concrete, and thus on the formation of the microstructure and consequently on the final mechanical properties and the durability of the SCC mixtures.

A considerable research effort is put in understanding and controlling these effects. Numerous sources focus on different aspects and parameters that affect the properties of SCC with a wide range of experimental techniques, trying to capture every aspect of the various occurring phenomena. For example, the effect of mineral additions, more specifically limestone additions and fly ash, and superplasticizers is widely investigated, due to their intensive use and important expected influence on the hydration [3–10]. However, a major part of the altering of the processes due to these ingredients happens in the first hours after mixing. Apart from temperature measurements, little possibilities existed up to recently to follow the early-age hydration continuously and with enough sensitivity for the diverse processes to be investigated. The Vicat-needle test sure is useful, but lacks sensitivity outside the setting stage and only allows a semi-continuous follow-up [11].

Ultrasonic testing methods are known to be very sensitive for microstructural changes in materials. Useful results can be obtained with reflection methods [12–14] and with transmission (UT) methods [13, 15]. Extending these methods with a continuous driver and data acquisition system allows a thorough follow-up of the earliest phases of the hydration of a concrete mixture. Several devices using the transmission method have been designed for this purpose and have proven their utility in uncovering the processes occurring before and during the setting and during the early hardening of different concrete compositions [16–20]. The fact that the UT method can be used while the concrete mechanically still behaves as a complex suspension as well as during the gradual formation of the elastic solid framework opens numerous new research possibilities. It is clear that this method can help clarify the influence of the complex composition of SCC on its early hydration and ultimately, on its hardened properties. The UT method has already shown its usefulness in clarifying the hydration behavior of different cement paste, mortar and concrete compositions in several research projects [5, 15, 21, 22].

The effect of the hydration on the p-wave velocity is subjected to a large number of variables. Distinction needs to be made between the behavior of the concrete as a suspension and as a porous solid. In both states, the p-wave velocity depends on the proportions and the elastic properties of the constituent materials, as well as the frequency of the propagating wave. Before the formation of the percolated microstructure, the concrete is a suspension of the aggregates and non-reacted powder (= cement + mineral addition) particles in the gradually hydrating cement paste, for which several authors have proposed adequate formulae for calculating the wave propagation velocity [23, 24]. The gradual change in the properties of the different fractions of the suspension, as well as their proportions causes a gradual rise of the p-wave speed.

The influence of the entrapped air bubbles cannot be neglected and induces a drastic drop of the p-wave speed, leading to velocities down to 100 m/s for air contents around 1% [25, 26]. After the formation of a percolated structure, the concrete can be considered as a partially saturated porous solid, in which the p-wave velocity can be determined using the Biot-Gassmann theory [25, 27]. The start of the increase of the penetration resistance in tests for the determination of setting time according to EN 196-3 and ASTM C 403 has been proven to be in good concordance with the inflection point in the p-wave velocity curve [11, 13, 14]. Various methodologies are presented to determine the start of the percolation, either relying on threshold velocities [19, 22, 28, 29] or on other p-wave curve characteristics. Robeyst [15] for example, calculates the age of the start of the ASTM C403 setting as 1.45 times the age at which the inflection point occurs, for a wide range of compositions.

Except for a few of the mixtures investigated in [15], little research has been done on the use of continuous ultrasonic testing on SCC. The use of diverse calorimetric methods is however well spread and has been used extensively to follow the heat of hydration of SCC mixtures [2, 8, 30–32] and allows determining the effects of the additions and admixtures on the hydration kinetics. The evolution of the heat of hydration gives a continuous view on the overall chemical reaction in the cementitious mixture, while setting and percolation are mechanical properties of the microstructure. Both characteristics are however intensely related. The penetration

resistance, on which the definition of setting is based, relies on the shear resistance of the mixture [33], which is in its turn related to the amount of interconnected hydration products [34]. This microstructural development can be expressed as a degree of hydration, which is easily determined by calorimetric measurements. As a consequence, it makes sense to relate the mechanical process, which can be described by ultrasonic testing, to the degree of hydration or to the heat of hydration itself. Schindler [35] proposes thresholds for the start and the end of the setting, based on the degree of hydration and the water-to-cement ratio (W/C), while Zingg [36] relates the start of the setting to a threshold in the heat production rate of the hydration.

The aim of this research is to determine the influence of the admixtures and additions in SCC mixtures on the evolution of the p-wave velocity and the heat of hydration of the mixtures. While the continuous ultrasonic tests will be performed on concrete mixtures, isothermal calorimetric tests will be performed on corresponding mortar mixtures. The start of the percolation and the end of the setting will be determined using both evolutions and relying on a number of methodologies. By comparing the results based on the established calorimetric test with the continuous ultrasonic test, the meaningfulness of the latter will be assessed in the specific case of self-compacting mixtures.

2 Materials and test methodology

2.1 Mix design

In this research, the hydration behavior of eight self-compac-ting concretes (SCC) and one traditionally vibrated concrete (TC) is analysed with the continuous ultrasonic p-wave test method. Table 1 shows the composition of these mixtures and the results of the conventional (non-ultrasonic) tests on fresh concrete. The self-compactability of the SCC mixtures has been obtained using a combination of a mineral addition and a third generation polycarboxylate ether (PCE) SP. While the composition of the mixtures has been fixed as to be able to study the influence of one component at a time, the quantity of superplasticizer has been adjusted to obtain a comparable self-compactibility for all mixtures. This feature will show to be of major importance for the interpretation of the results of the experiments. As such, the influence of the type of mineral addition, the type of PCE, the type of cement, the W/C and the cement-to-powder ratio (C/P, with powder P = cement + addition) will be compared as independently as possible, while maintaining an SCC with a similar, realistic, workability. SCC20 will be considered as the standard SCC mixture, to which all other mixtures will be compared.

In all the SCC mixtures, a constant amount of powder (600 kg/m^3) is used. In concretes SCC20 to SCC23, the mineral addition type is changed, while the amount of mineral addition (240 kg/m^3) remains equal. Two types of limestone addition, one quartz addition (Q) and one F-type fly ash (FA) are used in the experiments. The limestone additions have different grading curves, the limestone addition 1 (L1) being coarser than limestone addition 2 (L2). Figure 1 shows the grading curves of the different mineral additions, while their specific masses and Blaine fineness are listed in Table 2. PCE1 is replaced by PCE2 in mixture SCC24. Both SP's are watery solutions of their dry active PCE component: PCE1 is a 35% solution, while PCE2 is a 40% solution. Despite the small change in concentration, other tests [37] have shown that PCE2 has a significantly higher plasticizing effect. The exact chemical composition and molecular structure of both SP's is unknown, due to the producing company's trade secret policy.

In concrete SCC25, the Portland cement CEM I 52.5 R HES (CEM I) is replaced in equal amount by a coarser blast furnace slag cement CEM III/A 42.5 N LA (CEM III). Figure 2 shows the grading of both cements. Table 3 shows the chemical composition of both cements and their mineral composition, calculated according to the Bogue equations. The total theoretical hydration heat H_{cem} of CEM I is 478 J/g, calculated according to [38]. In mixture SCC26, part of the cement is replaced by limestone addition 1, maintaining the water-to-powder ratio W/P while lowering the C/P. In concrete SCC27, a higher amount of water is added, causing a higher W/C and W/P (in this case, a lower amount of SP was needed in order to obtain a comparable workability to SCC20). Finally, the traditionally vibrated concrete mixture TC20 has been tested, having the same W/C as the majority of the SCC mixtures. Several other

Table 1 Concrete mixture composition, fresh (non-ultrasonic) properties and 28 day cube compressive strength

	Unit	SCC20	SCC21	SCC22	SCC23	SCC24	SCC25	SCC26	SCC27	TC20
River gravel 4/14	(kg/m^3)	698	698	698	698	698	698	698	698	1,225
River sand 0/5	(kg/m^3)	853	853	853	853	853	853	853	853	640
CEM I	(kg/m^3)	360	360	360	360	360	–	300	360	360
CEM III	(kg/m^3)	–	–	–	–	–	360	–	–	–
L1	(kg/m^3)	240	–	–	–	240	240	300	240	–
	(Vol.%)	8.89	–	–	–	8.89	8.89	11.11	8.89	–
L2	(kg/m^3)	–	240	–	–	–	–	–	–	–
	(Vol.%)	–	8.86	–	–	–	–	–	–	–
Q	(kg/m^3)	–	–	240	–	–	–	–	–	–
	(Vol.%)	–	–	9.09	–	–	–	–	–	–
FA	(kg/m^3)	–	–	–	240	–	–	–	–	–
	(Vol.%)	–	–	–	10.21	–	–	–	–	–
Water	(l/m^3)	165	165	165	165	165	165	165	198	165
PCE1	(m% C)	1.25	1.39	1.39	1.88	–	0.97	1.25	0.69	–
	(kg/m^3)	4.50	5.00	5.00	6.75	–	3.50	3.75	2.50	–
PCE2	(m% C)	–	–	–	–	1.39	–	–	–	–
	(kg/m^3)	–	–	–	–	5.00	–	–	–	–
W/C	(–)	0.46	0.46	0.46	0.46	0.46	0.46	0.55	0.55	0.46
C/P	(–)	0.6	0.6	0.6	0.6	0.6	0.6	0.5	0.6	1.0
W/P	(–)	0.28	0.28	0.28	0.28	0.28	0.28	0.28	0.33	0.46
Slump flow	(mm)	836	797	855	857	867	788	820	723	–
Flow test	(mm)	–	–	–	–	–	–	–	–	334
Fresh air content	(%)	1.1	1.3	1.0	1.6	1.2	1.9	1.4	1.4	2
Specific weight	(kg/m^3)	2,375	2,385	2,360	2,320	2,375	2,330	2,375	2,335	2,375
$f_{c,cub,28d}$	(MPa)	84.3	87.0	93.2	99.1	79.1	64.1	74.1	62.9	62.6

properties of the same set of mixtures have been tested in the framework of an inter-universitary project. The results of these tests and more details regarding these mixtures can be found in [39, 40, 41, 37].

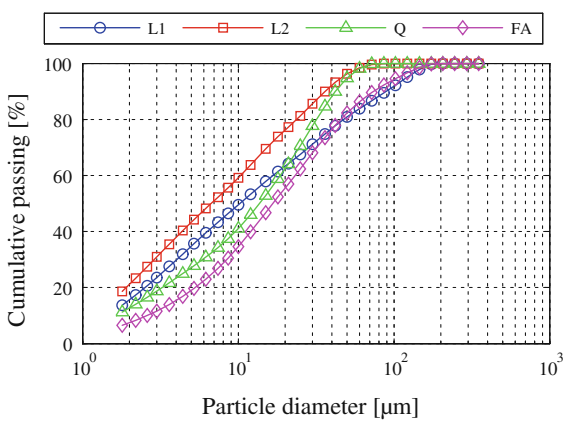

Fig. 1 Mineral additions grading

The isothermal calorimetry tests are performed on self-compacting mortar mixtures that are identical to the concrete mixtures described above where the gravel fraction has been left out. They are labelled SCM20 to SCM27 and TM20. The gravel fraction has not been replaced by sand or addition. As a consequence, W/C, C/P and W/P of the mortar mixtures are identical as their corresponding concrete mixtures. All considerations mentioned above for the concrete are also valid for the mortars. Table 4 indicates their composition for one unit batch and the result of a flow test.

2.2 Continuous ultrasonic test setup, procedure and data analysis

The ultrasonic testing device used in this research is the multi-channel IP-8, manufactured by Ultratest GmbH [42]. The device, as shown in Fig. 3, consists

Table 2 Specific mass and Blaine fineness of the aggregates, the cements and the mineral additions

	Specific mass (kg/m^3)	Blaine fineness (m^2/kg)
River gravel 4/14	2640	–
River sand 0/5	2640	–
CEM I	3280	540
CEM III	3030	471
L1	2700	338
L2	2710	558
Q	2640	388
FA	2350	346

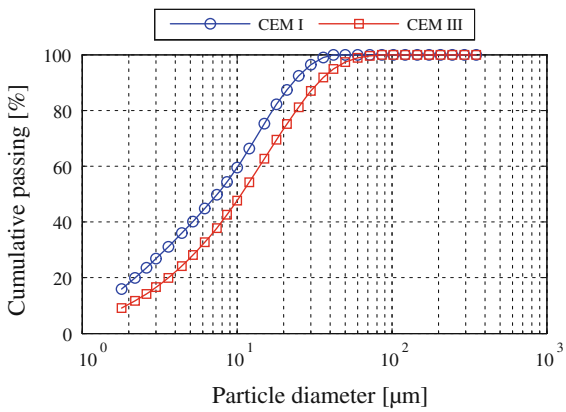

Fig. 2 Cement grading

of a PC-connected controller allowing up to eight simultaneous measuring channels, two of which are used in this research. Each measuring channel is composed of a cylindrical flexible silicone mould and an ultrasonic sender and receiver pair. The mould can hold cylindrical concrete or mortar samples measuring up to 70 mm across and 60 mm high, for a maximum sample volume of 230 ml. This volume is rather limited, but it results from a compromise between the representativity of the sample and the acceptable signal-to-noise ratio of the received signal, which is in direct relation with the sender to receiver distance. It is clear that for testing concretes with larger aggregates, this sample volume is not acceptable.

The mould allows the lateral fitting and fixing of the sender-receiver pair, in direct contact with the fresh concrete or mortar sample, for the measurement of the ultrasonic wave transit time in through-transmission. All tests are performed with a sender-receiver distance of 50 mm ± 5 mm. To ensure an optimal contact quality and an improved signal-to-noise ratio, as well as to avoid demoulding problems, the inside of the moulds and the contact surface of the ultrasonic testers are covered with a thin layer of spray-on silicon grease. The sample is sealed from the air with a silicone-fixed cover, thus avoiding excessive water evaporation and reducing drying shrinkage, which can lead to a loss of the contact of the sample with the ultrasonic testers. Figure 4 shows a detail of the silicon mould with the sender-receiver pair.

The p-wave narrow-band ultrasonic testers have a flat contact surface with the sample, measuring 25 mm in diameter and a resonant frequency of 25 kHz, which makes them well adapted for testing fresh concrete and mortar. Indeed, [16] shows the high transmission ratio of the low range of ultrasonic frequencies for concretes at very early age. Figure 5 shows the frequency transmission ratio of SCC23 as a function of concrete age. The transmission ratio is normalized for each concrete age. This data was

Table 3 Chemical composition (%) of the cements and the additions

	CaO	$CaCO_3$	SiO_2	Al_2O_3	Fe_2O_3	MgO	Na_2O	K_2O	SO_3	LOI[a]	C_3S	C_2S	C_3A	C_4AF
CEM I[b]	64.0	–	20.6	4.5	2.8	1.8	0.3	0.7	3.4	0.5	60.1	16.1	7.2	8.5
CEM III[b]	52.7	–	26.2	7.3	2.3	5.2	0.3	0.5	3.2	2.1	–	–	–	–
L1	–	98.1	0.6	0.2	0.08	0.35	<0.04	–	0.05	–	–	–	–	–
L2	–	97.2	–	–	–	–	–	–	0.002	–	–	–	–	–
Q[b]	<0.09	–	>98.5	–	<0.1	–	0.01	0.08	<0.005	0.13	–	–	–	–
FA[b]	4.6	–	48.0	28.6	7.2	1.1	0.4	1.2	1.8	4.9	–	–	–	–

[a] Loss on ignition at 975°C

[b] Determined according to EN 196-2 by means of XRF spectroscopy

Table 4 Mortar mixture composition and flow test results

	Unit	SCM20	SCM21	SCM22	SCM23	SCM24	SCM25	SCM26	SCM27	TM20
Standard sand EN196-1	(g)	853	853	853	853	853	853	853	853	640
CEM I	(g)	360	360	360	360	360	–	300	360	360
CEM III	(g)	–	–	–	–	–	360	–	–	–
L1	(g)	240	–	–	–	240	240	300	240	–
L2	(g)	–	240	–	–	–	–	–	–	–
Q	(g)	–	–	240	–	–	–	–	–	–
FA	(g)	–	–	–	240	–	–	–	–	–
Water	(g)	165	165	165	165	165	165	165	198	165
PCE1	(g)	4.50	5.00	5.00	6.75	–	3.50	3.75	2.50	–
PCE2	(g)	–	–	–	–	5.00	–	–	–	–
W/C	(–)	0.46	0.46	0.46	0.46	0.46	0.46	0.55	0.55	0.46
C/P	(–)	0.6	0.6	0.6	0.6	0.6	0.6	0.5	0.6	1.0
W/P	(–)	0.28	0.28	0.28	0.28	0.28	0.28	0.28	0.33	0.46
Flow test	(mm)	295	322	346	319	343	344	323	292	–

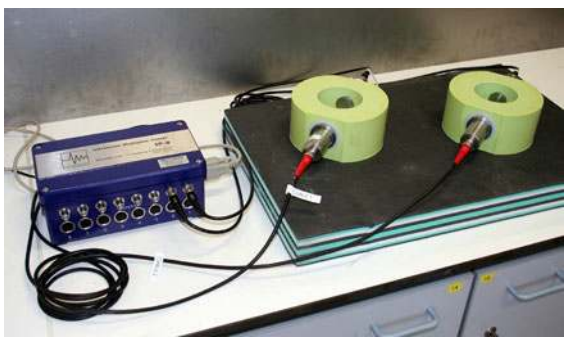

Fig. 3 The complete multi-channel IP-8 continuous ultrasonic testing device in a 2-channel setup

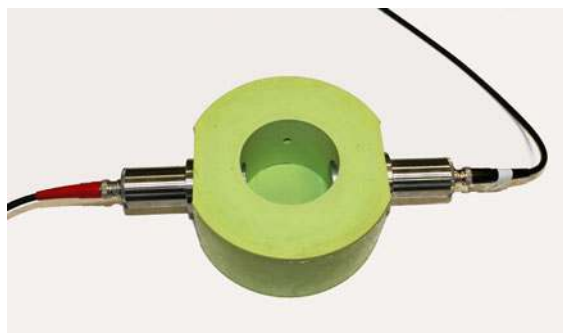

Fig. 4 Close-up of one measuring channel, showing the silicon mould, and the sender–receiver pair

acquired in a parallel continuous ultrasonic measurement, performed with the FreshCon testing device, developed at the University of Stuttgart. More details regarding this device can be found in [13, 16]. Contrary to the IP-8 setup, FreshCon uses a pair of broadband ultrasonic testers with a resonance frequency of ±0.5 MHz and a bandwidth of ±1 MHz. The frequency transmission ratio $\hat{R}_{\mathrm{Tr}}$ is calculated at every concrete age as

$$\hat{R}_{\mathrm{Tr}}(\omega) = \frac{\hat{U}_{\mathrm{conc}}(\omega)}{\hat{U}_{\mathrm{direct}}(\omega)} \quad (1)$$

where $\hat{U}_{\mathrm{conc}}(\omega)$ is the discrete Fourier transform of the time history of the received ultrasonic signal, that has passed through the concrete sample, and $\hat{U}_{\mathrm{direct}}(\omega)$ is the discrete Fourier transform of the time history of the received ultrasonic signal in the case when the sender and receiver have been placed in direct contact.

Even though the signal-to-noise ratio is very low up to 75 min, Fig. 5 clearly shows that during the first 100 min after the addition of the water, only frequencies under 25 kHz are transmitted through the fresh concrete. It is only after more than 200 min that a significant part of the frequencies over 100 kHz are transmitted to the receiver. At higher ages, high transmission ratios do still occur for small frequency bands around 23 and 34 kHz. This behavior is representative for the mixtures in this test program. It shows that an ultrasonic test circuit with a resonant frequency of 25 kHz is well suited for following the evolution of the p-wave propagation velocity through

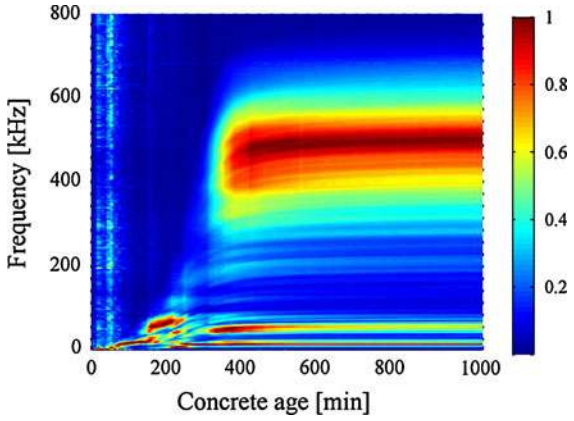

Fig. 5 The frequency transmission ratio $\hat{R}_{\mathrm{Tr}}$ for SCC23 as a function of concrete age and frequency

the hydrating concrete, by using a frequency band that has a significantly high transmission ratio throughout the entire test.

The device is programmed and controlled by the WinUltraSonic/IP-8 software application. Each received ultrasonic signal is filtered with a band-pass filter with a passband from 40 Hz to 100 kHz. The transmission time is measured with a precision of 0.1 μs, using a threshold onset picking algorithm to determine the arrival time of the signal. This threshold is set to 4 times the average noise level of the received signal. Up to this point, all data analysis, the filtering and picking of the arrival time, are set by the manufacturer of the IP8 and cannot be adapted by the user. The measured transmission time as a function of the concrete age is the only output of the device. Due to the flexible nature of the mould, the exact sender-to-receiver distance can only be measured on the hardened sample, at the end of the test and after demoulding. With this final measurement, the p-wave through transmission velocity can be calculated.

For each batch of each concrete mixture described in Table 1, 1 or 2 IP8 channels are used. After the mixing operation, as described in Sect. 2.4, the moulds are filled to the rim and closed as quickly as possible. The ultrasonic test is started immediately, in order to reduce the blind time interval of the test, in which the p-wave velocity is not being monitored. This interval is generally between 15 and 20 min long and is taken into account during the treatment of the data. It has no influence on the measurements in this study, since hardly any variations in the wave speed are measured during the first 30 min after the adding of the mixing water.

The wave propagation velocity is expected to change rapidly during the first 12 h of the hydration, while it tends to stabilize gradually after the end of the setting. It is therefore advisable to provide a higher sampling rate during the first hours of the experiment, to be able to catch the detail of the rapidly evolving concrete properties. After the stabilization, a longer interval in between two measurements still guarantees a correct monitoring of the wave speed, while it allows reducing the amount of data to process. In this experiment, data problems are not an issue, and the through-transmission time is measured every minute, throughout the entire experiment.

When the time histories of the p-wave velocities in all channels (i.e. all channels for the different batches of the same mixture) have been determined, the average p-wave velocity is calculated for each concrete age. A higher-order polynomial is fitted to this average velocity curve. The order of the polynomial is optimised to obtain an root mean squared error (RMSE) <10 m/s. The order of the polynomial ranges from 12 to 25, dependending on the mixture. This fitted curve is used for all further data analysis. Figures 6 and 7 illustrate an example of this procedure for SCC23. Figure 6 shows the 4 p-wave velocity developments for the four tested samples of SCC23 with the averaged p-wave velocity. Figure 7 shows the same averaged p-wave velocity curve, superposed on the 16th order polynomial fit, with an RMSE of 5.4 m/s. The RMSE is shown per

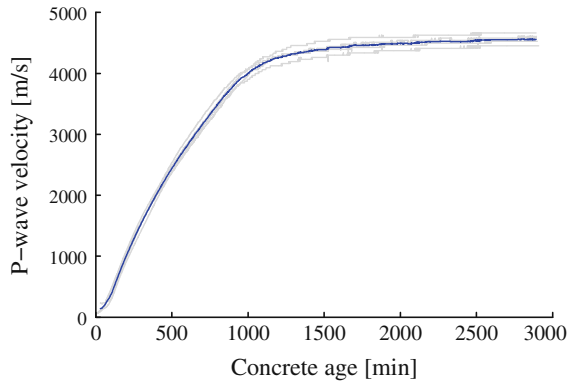

Fig. 6 Time history of the p-wave velocity of the individual SCC23 samples (*grey*) and of the mean p-wave velocity (*blue*)

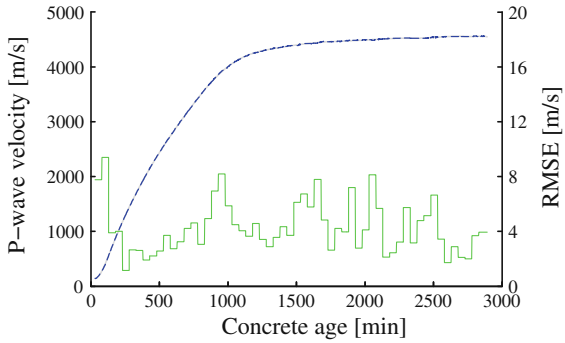

Fig. 7 On the left *Y*-axis: Time history of the mean p-wave velocity (*blue dashed*) and the 16th order polynomial fit to this curve (*grey*). On the right *Y*-axis: Time history of the running RMSE of the fit, per 50 min (*green*)

block of 50 min on the right *Y* axis, showing that even locally, the committed error never exceeds 10 m/s. Finally, the numerical derivative of the fitted p-wave velocity evolution is calculated as a function of time, using a first order centered difference algorithm. In what follows, the time history of this derivative will be referred to as the gradient of the p-wave velocity evolution.

2.3 Isothermal calorimetry test setup and data analysis

The evolution of the isothermal heat of hydration is determined using a Thermometric 3114/3236 TAM Air isothermal heat conduction calorimeter, at a constant temperature of 20°C. The tested mortar samples are taken out of a larger mortar batch, composed as in Table 4 and mixed as in Sect. 2.4. The weight of these samples is chosen so that each sample contains approximately 5 g of cement.

Immediately after the mixing procedure, a sample of each mixture is sealed in a designated 20 ml flask and placed in the calorimeter, after which the test is started. The blind period of the test (between the adding of the mixing water and the start of the acquisition of the heat flow) remains on average limited to 11 min. As a consequence, at least a part of the first hydration peak can be observed in the heat of hydration curves. The heat production is measured every minute. The experiment is continued for 7 days and the result is presented as the rate of the heat production as a function of time, per unit of cement, $q(t)$ (J/gh). The time history of the cumulative heat production per unit of cement $Q(t)$ (J/g) is then calculated as

$$Q(t) = \int_0^t q(t)\mathrm{d}t \tag{2}$$

Finally, the time history of the reaction degree $r(t)$ can be calculated as the ratio of the cumulative heat of hydration that has been released at any moment in time and the maximum cumulative heat $Q_{\max}$, obtained after 7 days, at the end of the test [28, 43]

$$r(t) = \frac{Q(t)}{Q_{\max}} \tag{3}$$

For the TC mixture and the SCC mixtures with a limestone addition and CEM I 52,5 R HES, the ultimate degree of hydration α_u calculated according to Mills' formula [44]

$$\alpha_u = \frac{1.031 \cdot (\mathrm{W/C})}{0.194 + (\mathrm{W/C})} \tag{4}$$

can be compared to the experimental hydration degree α_{exp} at 7 days,

$$\alpha_{exp} = \frac{Q_{\max}}{H_{cem}} \tag{5}$$

where H_{cem} is the total theoretical hydration heat of the cement for CEM I 52.5 R HES. Poppe [7] shows that Mills' formula is valid for limestone and quartz addition based SCC and SCM mixtures. Since this is not the case for fly ash based SCC, nor for the CEM III/A 42.5 N LA, α_u can not be calculated for these mixtures.

2.4 Mixing procedure and testing

2.4.1 Concrete mixtures

Of each concrete composition in Table 1, 3 or 4 mixtures of 25 l are prepared, which leads to a total of 4 to 6 tested samples for each mixture. All the concrete mixtures are prepared in a planetary pan mixer. The aggregates are oven-dried at 105°C and allowed to cool down to room temperature before the start of the procedure. During the first 15 s of mixing, tap water at a temperature of 20°C is added. 1 min later, the mixing is stopped for 15 s, during which the SP is added to the concrete. Mixing continues for another 2 min, after which the experiments can be started.

Apart from the ultrasonic monitoring as detailed in Sect. 2.2, three other tests are performed on the fresh concrete. The slump flow of the fresh SCC mixtures is determined, as well as the density, according to EN 12350-6, and the air content, using the pressure gauge method, according to EN 12350-7. For the TC, the slump flow test is replaced by a flow table test according to EN 12350-5. The results of these tests are presented in Table 1. The remaining part of the concrete is cast into 150 × 150 × 150 mm^3 cubes and used to determine the compressive strength at 28 days.

2.4.2 *Mortar mixtures*

One 0.7 l batch of each mixture is prepared for every mortar composition of Table 4. Because of the presence of the additions and the SP, the standardised mixing procedure according to EN 196-1 can not be followed. While maintaining the standardised mixing speeds, the following procedure is used: All dry components (cement, sand, addition) are placed in the mixing bowl and mixed at slow speed for 75 s. All the water is added during the first 15 s of this 75 s. The mixer is then stopped for 45 s, during which the SP is added to the paste and after which mixing continues at high speed for 60 s. The mixer is then stopped for another 30 s and the mixture is left to rest. Finally, mixing continues for another 120 s at low speed. Immediately after the mixing, the isothermic calorimetry test is started, as described in Sect. 2.3. With the remaining mortar, the consistency (by flow table) is determined according to EN 1015-3. The results of this test are indicated in Table 4.

3 Continuous ultrasonic monitoring: results and discussion

The time history of the p-wave velocity and the gradient of the p-wave velocity are examined for each mixture. A number of thresholds and characteristic points in the p-wave velocity and gradient curve are also considered in the analysis: A p-wave velocity of 1500 m/s (approximately the p-wave velocity in water) is found by several authors [19, 22, 29] to be a good indicator of the initial setting of traditionally vibrated mortar mixtures, as determined by penetration resistance tests. Robeyst [15] finds a good correlation between this initial setting and the mortar age at which the inflection point (i.e. the maximum of the gradient) in the p-wave velocity curve occurs, multiplied by 1.45.

This same inflection point is found to be an indicator of the start of the penetration resistance in ASTM C403 tests [14, 19]. According to Herb [28], a p-wave velocity of 2975 m/s provides a good estimate of the end of the setting, as determined by a ASTM C403 penetration resistance test for a wide range of mixtures. Robeyst [15] relates this end of the setting to the age of the concrete at which the p-wave velocity gradient has descended to 20% of its maximum value, and the p-wave velocity curve starts to flatten out. Except for a limited number of examples in the work of Robeyst [15], where different SP's are combined with fly ash, these relationships have not yet proven their validity in the case of SCC or SCM mixtures. The two thresholds and two characteristic points are here used to demonstrate the differences between the different mixtures. In Sect. 5, their meaningfulness will be investigated by a comparison to the results of the isothermal heat of hydration tests.

The fact that the quantity of superplasticizer has been adjusted to obtain a comparable self-compactibility for all mixtures results causes some trouble when assessing the effect of the change of the main parameters on the p-wave velocity. A true parametric study of the effect of the SP on the delay of the inflection point in self-compacting mortars is performed in [45], on mortar mixtures using limestone addition 1 and PCE1. It is shown that, within a common mortar consistency range, a linear relationship exists between the concentration of PCE1 and the delay of the inflection point of the p-wave velocity curve. For a SCM with $C/P = 0.65$ and $W/C = 0.45$, a PCE1 concentration rise of 1 mass% of the cement results in a supplementary delay of ±100 min. While this result cannot be entirely extrapolated to the compositions in this research, it is a good indicator of the order of magnitude of the expected influence of PCE1 on the delay of the inflection point. This influence can be as small as 14 min, between SCC20 and SCC21, for example, or as big as 119 min between SCC27 and SCC23.

Figure 8 shows the p-wave propagation velocity (m/s) on the left and the p-wave velocity gradient

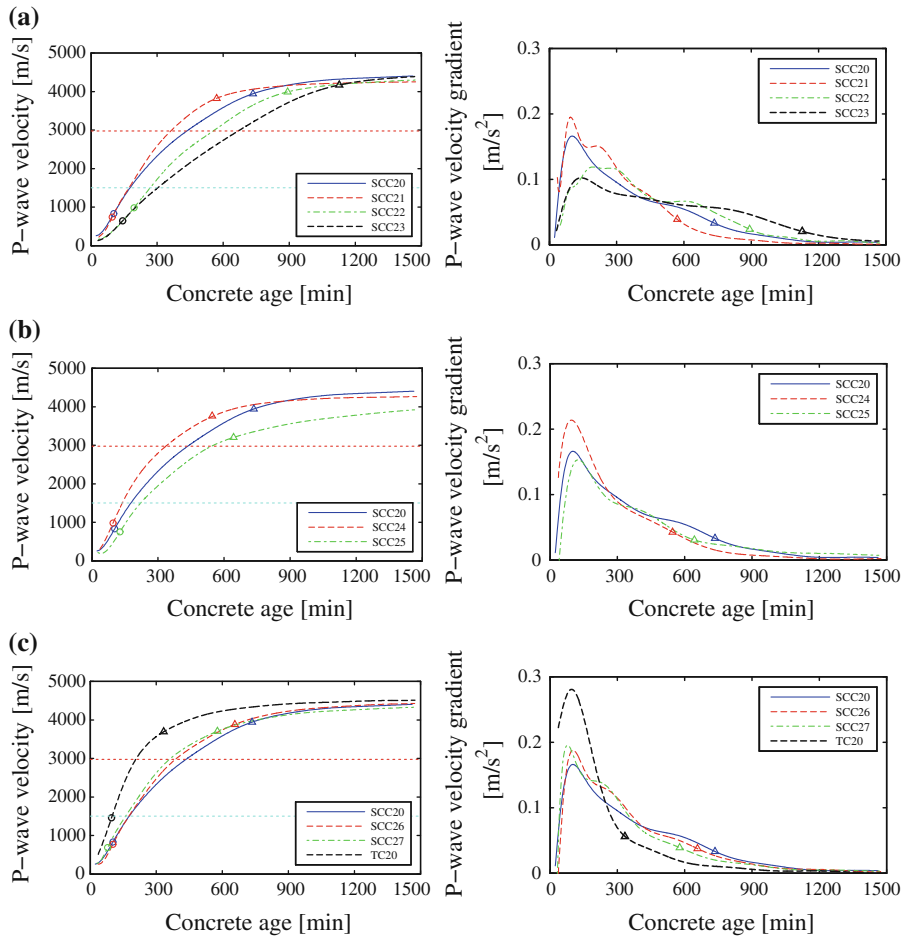

Fig. 8 p-Wave velocities (m/s), 1500 m/s (*blue dashed horizontal*), 2975 m/s (*red dashed horizontal*) threshold, the inflection point (*circles*) and the 20% of the maximum gradient point (*triangles*) (*left*) and gradients (m/s^2) and the 20% of the maximum gradient point (*triangles*) (*right*) as a function of concrete age (min), for the different mixture groups

(m/s^2) on the right, both as a function of time, for all mixtures, divided in three groups. SCC20 is the reference mixture, to which all other eight mixtures are compared and is repeated in each group. The time (in minutes) on the axis starts at the moment of the addition of the water to the concrete. Both p-wave velocity thresholds, the inflection point and the point at which the p-wave velocity gradient has descended to 20% of its maximum value are indicated on the velocity graphs. Only this final point is shown on the gradient graphs.

Table 5 shows the overview of the concrete ages for the thresholds and characteristic curve points, as well as the maximum gradients of the p-wave velocity curves.

3.1 SCC20 vs. SCC21 (Fig. 8a)

Both mixtures initially show a practically coinciding p-wave velocity evolution, with a slightly earlier inflection point for SCC21. Both velocity curves diverge after 3 to 4 h, once the 1500 m/s threshold has been passed, because of a higher velocity gradient for SCC21. While the ultimate p-wave velocities are very similar, the SCC21 velocity curve does flatten out much earlier. Because of the higher quantity of SP present in mixture SCC21, a deceleration of the p-wave velocity and a delayed start of the setting could be expected [2, 15]. Both effects are apparently compensated due to the more intense acceleration of the hydration caused by the

Table 5 Maximal p-wave velocity gradient and selected p-wave velocity related key concrete ages, for all mixtures

Mixture	Maximal p-wave velocity gradient (m/s^2)	Concrete age (min) at			
		Inflection point	1500 m/s threshold	2975 m/s threshold	20% of maximum gradient
SCC20	0.17	103	177	435	735
SCC21	0.20	96	172	362	570
SCC22	0.12	195	270	540	875
SCC23	0.10	143	303	668	1127
SCC24	0.21	96	138	336	546
SCC25	0.15	127	221	543	643
SCC26	0.19	103	176	387	657
SCC27	0.20	79	161	360	578
TC20	0.28	97	125	207	334

finer limestone addition 2 used in mixture SCC21. This leads to a higher nucleation surface and a higher precipitation of the hydration products, as confirmed in [46, 47].

3.2 SCC20 vs. SCC22 (Fig. 8a)

The overall lower hydration velocity of SCC22 can be attributed to three competing factors: First of all, the inert but catalytic limestone addition is replaced by an inert quartz addition, which is not known to cause an acceleration or reduced dormant phase of the hydration [8]. The delaying effect of the quartz addition on the inflection point of the p-wave velocity curves of SCM is however clearly shown in [45], where replacing a limestone by a quartz addition causes delays up to 200 min for $C/P = 0.65$. The higher fineness of the quartz addition is less of an issue here, since these particles are not expected to act as a nucleation surface. There will however be more free water absorbed by the quartz addition, which might result in a less pronounced hydration. Since W/C is relatively high and the SP provides a good dispersion of the cement grains, this factor is not expected to affect the hydration rate. Secondly, a slightly larger amount of SP is used compared to SCC20, causing a supplementary retarding of the hydration reactions. Finally, the quartz addition has a lower specific mass, causing it to occupy a larger volume in the concrete mixture, for an equal mass added. This densifying effect is described in detail by Boel [48]. The denser microstructure causes a stiffer mixture, leading to a rise of the p-wave propagation velocity and an earlier formation of a percolated structure, partly compensating the previously mentioned effects.

3.3 SCC20 vs. SCC23 (Fig. 8a)

Changing the limestone addition by an equal mass of fly ash has an even more clear decelerating effect on the hydration, as also mentioned by [49]. The inflection is however not as delayed as compared to SCC22. Within the time frame of this test, fly ash is considered to be inert: the duration of the experiment is far too short to be able to observe its puzzolanic activity. Fly ash has however an influence on the hydration, lengthening the dormant period and most often lowering the rate of heat production, long before the start of the puzzolanic activity [2]. Because of the fact that a larger amount of SP is used, it is not self-evident to make a clear distinction between the effects of both modifications to this mixture: It is hard to say whether the slower formation of the microstructure is merely due to the absence of the nucleating surface effect of the limestone addition, or whether fly ash itself causes a supplementary deceleration, as mentioned in [50]. On top of that, the fly ash occupies a larger volume in the mixture (even more than in SCC22), which partly compensates for the lower wave velocity, as explained in Sect. 3. The slower initial formation of the microstructure is followed by a significantly more intense activity in SCC23 after 6 h of hydration. This might be related to the positive influence of the fly ash on the C_3A hydration as suggested by Baert [31]. However, this

effect is expected to occur later and is actually not being witnessed in the heat of hydration tests in Sect. 4. Finally, the fly ash has a comparable Blaine fineness as the limestone addition in SCC20, so that the water consumption of both additions and the related effect on the intensity of the hydration can thus be neglected.

3.4 SCC20 vs. SCC24 (Fig. 8b)

Replacing PCE1 with PCE2 leads to a considerable acceleration of the hydration reaction and a slightly earlier inflection point. Despite the fact that a larger mass of PCE2 is added to SCC24, the difference in the total mass of added active (dry) material between both PCE is minimal. The difference in the hydration can thus probably be attributed to the specific differences in the chemical composition of both superplasticizers (not known to the authors). This result also illustrates the fact that the SP not only has a major effect on age at which occurs the inflection point, but also on the acceleration of the p-wave velocity.

3.5 SCC20 vs. SCC25 (Fig. 8b)

Observing the p-wave velocity graph, the use of blast furnace slag cement CEM III/A 42.5 N LA instead of Portland cement CEM I 52.5 R HES results in a significantly slower and delayed hydration, as can be expected due to the lower reactivity of the BFS cement. It is known that the dispersion effect of PCE SP's is reduced in the presence of BFS cements [51], due to a higher sulphate content. Since the sulfate content in both cements is ± equal, this effect is not expected here. The lower amount of SP would, on itself, lead to less deceleration and an important reduction of the inflection point delay. Clearly, the reduced reactivity of the BFS cement is the predominant factor in this case. The large difference of the p-wave propagation velocity at 48 h is another result of the slower hydration of the blast furnace slag cement CEM III/A 42.5 N LA.

3.6 SCC20 vs. SCC26 (Fig. 8c)

The reduced C/P and the consequently higher W/C will influence the development of the microstructure in SCC26. The higher W/C is expected to cause a slower p-wave velocity evolution: Because of the higher dispersion of the cement grains, a higher degree of hydration is needed to obtain a connected solid volume fraction [19, 52], leading to a fast p-wave velocity increase. However, due to the changed proportions, the total solid volume is higher, leading to a slightly stiffer microstructure and higher p-wave velocities. The higher amount of limestone addition is likely to accelerate the occurring hydration reactions. A higher velocity gradient and an earlier flattening of the velocity curve are indeed noted for the SCC26. The acceleration effect of the hydration caused by the limestone addition is however also known to be less pronounced than normally in occurrence of a higher W/C [46]. This shows the prevalence of the effect of the mineral addition quantity. Overall, the combination of the different influencing parameters leads to two fairly similar wave propagation curves.

3.7 SCC20 vs. SCC27 (Fig. 8c)

Again, the effects of a number of phenomena combine into two very similar p-wave propagation velocity curves, except for a more reduced time to the inflection point. Furthermore, a slightly higher initial and maximum velocity gradient can be observed for SCC27. First of all, the higher W/C is expected to lead to lower p-wave velocities and gradients and extended delays, as mentioned before. The predominant factor in this mixture is however the significantly lower amount of SP, which causes the earlier start of the setting and less deceleration of the wave velocity, compared to the standard mixture. This last effect is partly countered by the lower acceleration of the hydration by the limestone addition in the presence of a higher W/C, as mentioned before.

3.8 SCC20 vs. TC20 (Fig. 8c)

The basic influence of the use of a limestone addition and PCE superplasticizer can be observed by comparing the traditionally vibrated concrete TC20 to the standard SCC20 mixture. SCC20 clearly shows a small delay in the p-wave velocity evolution, while the gradient of the p-wave velocity is inferior during the first 4 h of the hydration. This is again the result of a combination of effects.

The presence of the limestone addition generally has a tendency to reduce the dormant phase and

accelerate the early hydration reactions [8, 49, 50]. This acceleration can be explained by the fact that the finely ground limestone particles provide nucleation surfaces for the hydration products. The presence of a SP is known to cause both a delay of the start of the setting as well as a reduced hydration speed, due to different phenomena, as discussed in [39, 49]. Here, the SP deceleration effect clearly dominates the acceleration due to the limestone addition. The following comparisons give an extended insight in the proportions of these effects. It should furthermore not be neglected that, while the total mineral content (aggregates + mineral additions) in both mixtures is fairly equal, the aggregate content of the TC20 is much higher and the gravel-to-sand ratios of both mixtures are completely different, which results in a much altered aggregate packing. This alteration can change the initial gravitational densification after the casting of the concrete, which can alter the velocity gradient before the start of the percolation. It will also change the final packed state of the concrete which can result in a constant offset between the wave velocities.

3.9 Additional observations

For all mixtures, an almost immediate rise in the p-wave velocity can be noticed. The very rapidly reacting cement CEM I 52,5 R HES has a very short dormant period, but it is expected to end at least 45 min after adding the water [53]. Accelerating factors, as for example the presence of the limestone addition will influence the velocity changes, but they are not expected to cause the very early sound speed changes noticed in the experiments. A number of elements have been reported that can possibly contribute to this phenomenon.

First of all, the formation of ettringite in the concrete suspension, prior to the percolation threshold of the microstructure leads to a change in the compressibility of the suspension. While setting has not yet occurred, this will lead to a rise of the p-wave propagation speed [14]. It can be expected that the effect of pre-set activity on the p-wave velocity is more pronounced for SCC. Assuming the p-wave velocity through the gravel phase of the mixture does not change throughout the experiment, all velocity changes can be attributed to the paste. Due to the significantly larger paste content in SCC, the effect of changes in the paste will result in a more pronounced p-wave evolution for the complete mixture. The results of the TC20 mixture contradict this, which leads to suspect that the retarding effect of the SP is so dominant, that it overshadows out all other influences.

Robeyst [15] investigates a number of other possible influencing factors. First of all, internal gravitational settling can cause a densification of the mixture, which leads to a slight raise in the p-wave velocities in the first 48 h of the test. Furthermore, air bubble migration to the surface can have similar effects. Finally, the thixotropic behavior of a mixture tends to cause a supplementary p-wave velocity increase. All of these effects are however very small and slow, so that their individual influence will be hardly noticeable in the first hour of the hydration. Their combined effect, while difficult to detect, can however be more significant. The specific properties of self-compacting mixtures can have an influence, at least on the first two of these effects. Indeed, the increased fluidity in the presence of higher SP quantities can lead to faster settling and bubble migration.

Finally, the frequency band in which the IP8 device operates, guarantees the transmission of a maximal part of the energy in the pass band of the concrete at very young age [16], as illustrated in Fig. 5. This feature makes this device most suitable for the earliest observations and enables a swift response of the measuring system to even the slightest changes in the microstructure of the fresh concrete.

The relative importance and codependency of the different parameter and composition changes significantly influences the combined amplification or reduction of their effects on the measured p-wave velocity curves. The multitude of intervening factors in this research makes it hard to distinguish these effects in an unambiguous manner. While it allows comparing the early-age hydration behavior of differently composed SCC mixtures, the setup of this round of experiments is not ideal for the purpose of pinpointing the individual impact of each factor of influence.

4 Isothermal calorimetry: results and discussion

The time history of the heat production rate q (J/gh), obtained by an isothermal calorimetric test at 20°C and of the cumulative heat Q (J/g) calculated by Eq. 2,

Table 6 Q_{max}, q_{max} and selected heat production related key concrete ages, for all mixtures

Mixture	Q_{max} (J/g)	α_{exp} (–)	α_u (–)	q_{max} (J/gh)	Concrete age (min) at				
					q_{min}	q_{min} + 0.25 J/gh [36]	$r = 0.15 \cdot (W/C)$ [35]	q_{max}	$r = 0.26 \cdot (W/C)$ [35]
SCM20	378.9	0.79	0.73	19.62	209	265	123	677	388
SCM21	393.9	0.82	0.73	20.82	192	237	106	619	350
SCM22	423.2	0.89	–	22.61	203	249	87	682	350
SCM23	405.1	0.85	–	19.68	276	361	56	903	363
SCM24	415.6	0.87	0.73	23.03	152	189	121	531	311
SCM25	308.6	–	–	6.82	264	360	375	867	638
SCM26	434.4	0.91	0.76	21.81	190	235	173	600	398
SCM27	416.4	0.87	0.76	20.25	163	200	205	565	381
TM20	358.2	0.75	0.73	18.28	90	116	83	429	236

are examined for each mixture. A number of characteristic points are considered in the analysis and are indicated in Table 6. According to Zingg [36], the age at which $q = q_{min} + 0.25$ J/gh is proposed as a good measure for the start of the setting as determined by a Vicat penetration test, for mixtures containing PCE SP's. Schindler [35] shows that the reaction degrees $r_i = 0.15 \cdot (W/C)$ and $r_f = 0.26 \cdot (W/C)$, correspond respectively to the start and the end of the setting as determined by an ASTM C403 penetration test. The mortar ages at which $q = q_{max}$ and $q = q_{min}$ are also taken into consideration.

Table 6 shows the overview of the cumulated heat at 7 days Q_{max} (J/g), the maximum heat production rates q_{max} (J/gh), the experimental and ultimate hydration degree α_u and α_{exp}, respectively calculated according Eqs. 4 and 5, and the characteristic mortar ages mentioned above for all mixtures. The concrete age at $r_i = 0.15 \cdot (W/C)$ for mixtures SCM22 and 23 yields non-coherent results due to the fact that these two mixtures exhibit very high "wetting" peaks. While this causes only a minor set-off for the main part of the curve, it has a big influence on the age at which the lowest Schindler threshold is attained. Both results will be marked separately during the comparative analysis in Sect. 5.

Figure 9 shows, on the left, the first 48 h of the time history of the heat production rate q (J/gh) and on the right, the time history of the cumulative heat Q (J/g) for the different mixtures for the entire duration of the test. The mixtures are divided in the same three groups as in Sect. 3. SCC20 is again considered to be the reference mixture, to which all other eight mixtures are compared. The time (in minutes) on the axis starts at the moment of the addition of the water to the concrete. Since it is not being examined here, and to allow a better focus on the main part of the heat production curves, the wetting peak in the heat production rate curve is cut short at 25 J/gh.

First of all, it can be observed that the α_{exp} are particularly high, and for all mixtures except TC20, 10 to 15% above α_u as proposed by Mills. It seems the validation for SCC performed by Poppe [7] does not stand here. This increase in the heat production can be attributed to the PCE SP's used, mainly on the basis of the dispersive effect of the SP's, allowing an improved wetting of the individual cement grains and thus stimulating diffusion controlled hydration [15].

4.1 SCM20 vs. SCM21 (Fig. 9a)

The finer limestone addition 2 causes a slightly accelerated hydration, a higher q_{max} and a reduced induction period. The higher fineness results in a higher total granular surface, allowing a more important nucleation of the hydration products on the limestone particles. All curve parameters consistently bare the effect of this acceleration. None of both SCM's show a distinct third hydration peak. Not more than a hint of a shoulder can be observed for SCM20, around 800 min. This third peak can be related to the promotion of the hydration of C_3A by the presence of the assumedly inert limestone addition [2, 8]. The absence of this peak can be expected, given the low C_3A content of the cement and the low isothermal hydration test temperature. While the third peak is expected to be more

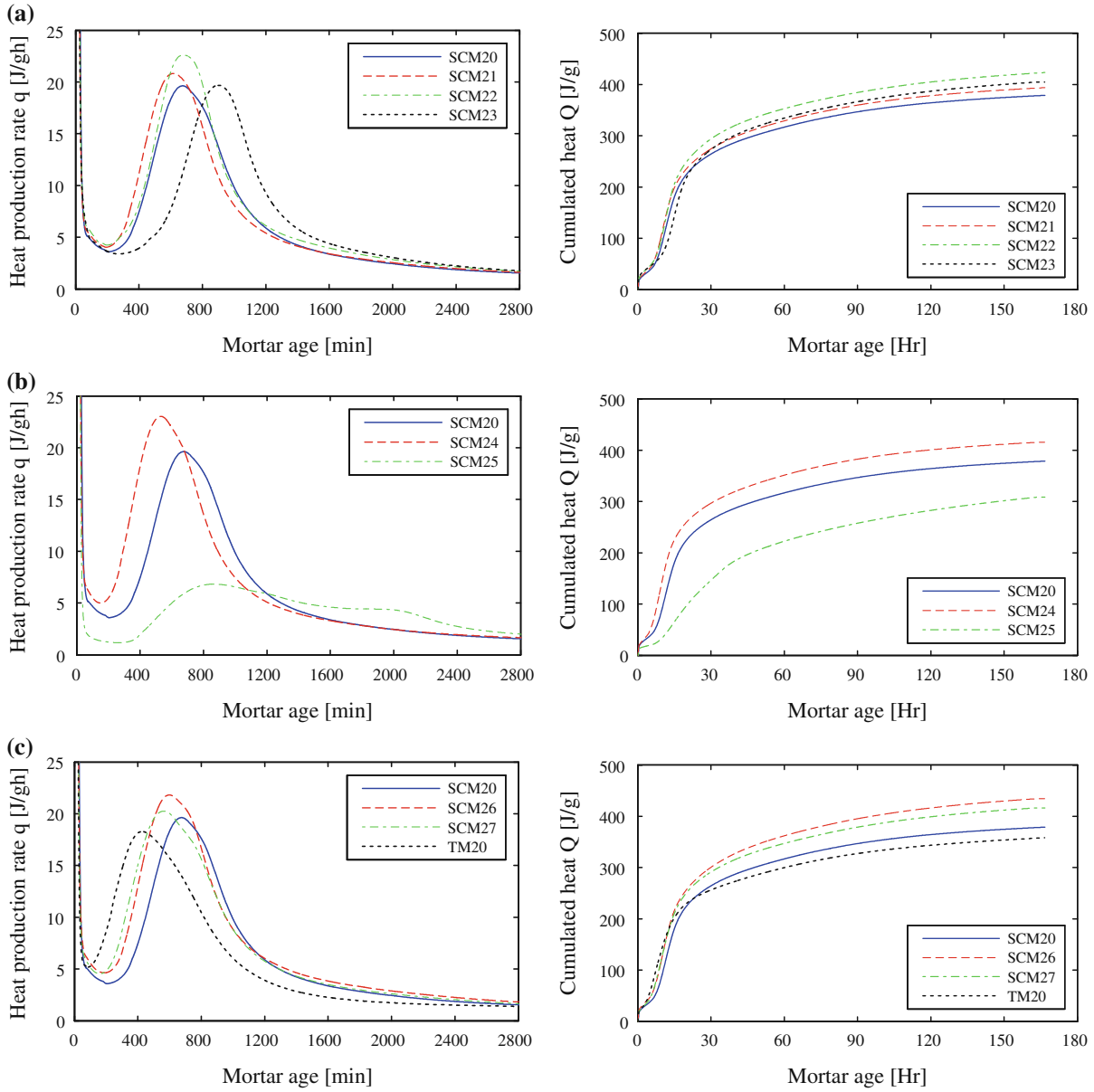

Fig. 9 Heat production rates q (J/gh) (*left*) and cumulated heat Q (J/g) (*right*), as a function of concrete age for the different mixture groups

pronounced for SCM22, due to the higher added volume and the higher specific surface, no such effect is noticed. This can be explained by the fact that the finer grading of the limestone addition 2 advances the third hydration peak, making it coincide with the second peak. A theory explaining these effects based on a hypothesis of a non-inert limestone addition is discussed in [2]. The higher amount of SP is expected to extend the induction period and increase q_{max} and Q_{max} even more [15]. This study does however not allow to make a distinction between the effect of the higher SP quantity and the changed limestone addition content.

4.2 SCM20 vs. SCM22 (Fig. 9a)

There is hardly any delay between the quartz (SCM22) and the limestone addition 1 based SCM

(SCM20), as can also be observed by the similarities in most curve parameters. While quartz is not expected to influence the hydration, the maximum heat production rate q_{max} of SCM22 is however significantly higher than that of SCM20 and SCM21, and so is the Q_{max}. This could be related to a nucleation effect, though no precedents have been encountered and the overall fineness of the Q addition is similar to that of limestone addition 1. The higher amount of SP could as well be an influencing factor, as mentioned above. With that in mind, one would however also expect to observe an extension of the dormant period, which is not the case. Furthermore, SCM21 contains the same amount of SP and does not show such a high raise of q_{max}. This clearly calls for further investigation.

4.3 SCM20 vs. SCM23 (Fig. 9a)

While the heat production rate of the FA-based SCM23 is much similar to that of SCM20, its induction period is significantly extended. This delay is typical for the presence of FA [2, 15, 54] and is reinforced here by the higher SP content, needed to maintain the self-compacting properties of the mixture. The rate of heat evolution and the height of the second peak in the presence of FA are depending on the specific FA used [2, 38] and can be higher or lower. Also, the higher SP content contributes to the height of q_{max}. The raise (compared to TCM) is thus perfectly acceptable. There is no evidence of a third peak in the heat production rate curve.

4.4 SCM20 vs. SCM24 (Fig. 9b)

Replacing PCE1 by PCE2 has an important effect: The dormant period is shortened and q_{max}, as well as Q_{max}, are much increased. As mentioned before, PCE2 has a higher dispersion effect, and is added in a slightly higher concentration. Despite this, the dormant period is shortened. This shortening is commonly attributed to two aspects [2]: the dispersion effect of the SP, which changes the hydration kinetics, and the adsorption of the SP molecules at the surface of the cement grains, which has an adverse effect on the diffusion of water and calcium ions. Since the dispersion effect of PCE2 is higher, its adsorption must be reduced by its different structure and chemical composition, causing the shortened dormant period. On the other hand, the heat production rate of SCM 24 is much higher, which is coherent with the higher dispersive effect of PCE2.

4.5 SCM20 vs. SCM25 (Fig. 9b)

When the CEM I 52.5 R HES is replaced by an equal quantity of a coarser compound CEM III/A 42.5 N LA, the effects on the development of the heat of hydration of SCM25 are important. The rate as well as the total heat of hydration is much lower, and the induction period is extended, due to the coarseness of the cement and the fact that it contains between 35% and 65% of BFS. Due to the additional reduction of the SP quantity, the extension of the dormant period and the decrease of the heat production rate have been partly mitigated. Finally, a third peak is clearly visible at ±35 h, most likely caused by the reaction of the BFS itself [11, 55].

4.6 SCM20 vs. SCM26 (Fig. 9c)

By replacing some of the cement by limestone addition 1, the C/P of SCM26 is brought to 0.5 and the W/C is raised to 0.55. Furthermore, the SP quantity is reduced to 1.25% of the cement mass. This causes a number of concurring effects on the hydration kinetics. The improved wetting of the cement will increase the heat production ratios, while the higher quantity of limestone addition 1 provides a larger nucleation surface for the hydrating cement, reducing the induction period and increasing heat production ratios. By reducing the SP quantity, it is expected to reduce the induction period and the reaction rate. Combining these effects, results in a higher q_{max} and Q_{max} and a significantly reduced induction period. Like for SCM20, the heat of hydration rate of SCM26 shows a small hint of a third peak, here caused by the lower C/P.

4.7 SCM20 vs. SCM27 (Fig. 9c)

In SCM 27, the necessary workability is obtained by adding water and reducing the SP content, resulting in a higher W/C. Again, two concurring effects will influence the hydration. Because of the much lower SP quantity, the induction period and the reaction rate are decreased significantly, compared to SCM20. The higher W/C will however result in an improved

wetting of the cement and will increase the heat production ratio. Together, these effects result in an even shorter induction period than in SCM26, though heat production rates are slightly lower. This is most probably due to the lower amount of limestone addition 1, compared to SCM26. Again, a small start of a third peak is visible. While this can also be observed in [8], no clear relationship with the higher W/C can be established.

4.8 SCM20 vs. TM20 (Fig. 9c)

Finally, the hydration of all SCM is delayed compared to the TM, even though most of them contain a limestone addition, known to reduce the induction period. This indicates the predominance of the retarding effect of the PCE SP, as was also observed in the results of the continuous ultrasonic tests. With regard to the heat of hydration rate, the limestone addition and the SP act together and cause such an increase in all SC mixtures, that TM has the lowest q_{max} of all mixtures, with exception of SCM25, containing the CEM III/A 42.5 N LA. This can be expected, because of the important BFS content of the compound cement in SCM25 and its significantly higher coarseness, compared to the CEM I 52.5 R HES.

5 Continuous ultrasonic monitoring versus isothermal calorimetry

The hydration process has been quantified using two very different test methods. The evolution of the p-wave velocity focusses on the mechanical aspects of the hydration, depending on the changes of the elastic properties of the mixture, which are directly related to the microstructural changes of the concrete or mortar. The evolution of the heat of hydration on the other hand, is a reflection of the chemical processes in the cementitious mixture. As detailed in Sect. 1, both are closely related. The results of each method have been characterised using a few well-chosen key concrete/mortar ages, related to the start and the end of the setting process. The overview of these ages is given in Tables 5 and 6. In Fig. 10 the correlation of the key concrete ages linked to the start of the hydration is investigated. The same is done in Fig. 11 for those ages related to the end of the setting process. Only linear correlations were investigated that have a y-intercept value = 0, assuming a constant ratio between two concrete ages, or that are parallel to the $y = x$ identity, assuming a constant delay between the two concrete ages.

5.1 Correlations with regard to the start of the setting (Fig. 10)

Generally, the TC20 and SCC/SCM22 show a distinctly different relationship compared to the other mixtures. They are not taken into account for the determination of the correlations. Also, apart from a few isolated mixtures, none of the UT-related concrete ages correlate well with the estimation of the start of the setting according to Schindler [35]. This indicates a different relationship between the reaction degree and the start of the setting for self-compacting mixtures, than the one proposed by Schindler.

Overall, good correlations can be found for q_{min} and at $q_{min} + 0.25$ J/gh, which corresponds to the start of the setting according to Zingg [36]. For the concrete age at the inflection point of the p-wave velocity curve this results in ratios of 1.94 and 2.49 and R^2 of 0.83.

Outside the main correlation group, there is a very good correspondence between the inflection point q_{min}, for TC20 and SCC/SCM22, without any correcting factor.

The best correlation with q_{min} can be obtained by multiplying the concrete age at which the inflection point of the p-wave velocity is obtained by 1.45, i.e. the start of the setting (ASTM C403) as indicated by Robeyst [15], with an R^2 of 0.87. The SCC age at the 1500 m/s p-wave velocity threshold is an indicator with a slightly lower R^2, but a good correlation can be obtained using a fixed, small delay of 14 min. The best correlation with $q_{min} + 0.25$ J/gh is obtained by adding 60 min to this 1500 m/s threshold concrete age.

The fact that the inflection point of the p-wave velocity curve of almost all SCC mixtures precedes the age at which q_{min} is reached, clearly illustrates the different nature of both processes: At a moment where the chemical activity of the mixture is at its low point, the microstructural formation is at its maximum rate. This indicates again that other factors, apart from hydration, are involved in the evolution of the p-wave velocity, as already detailed in Sect. 3.

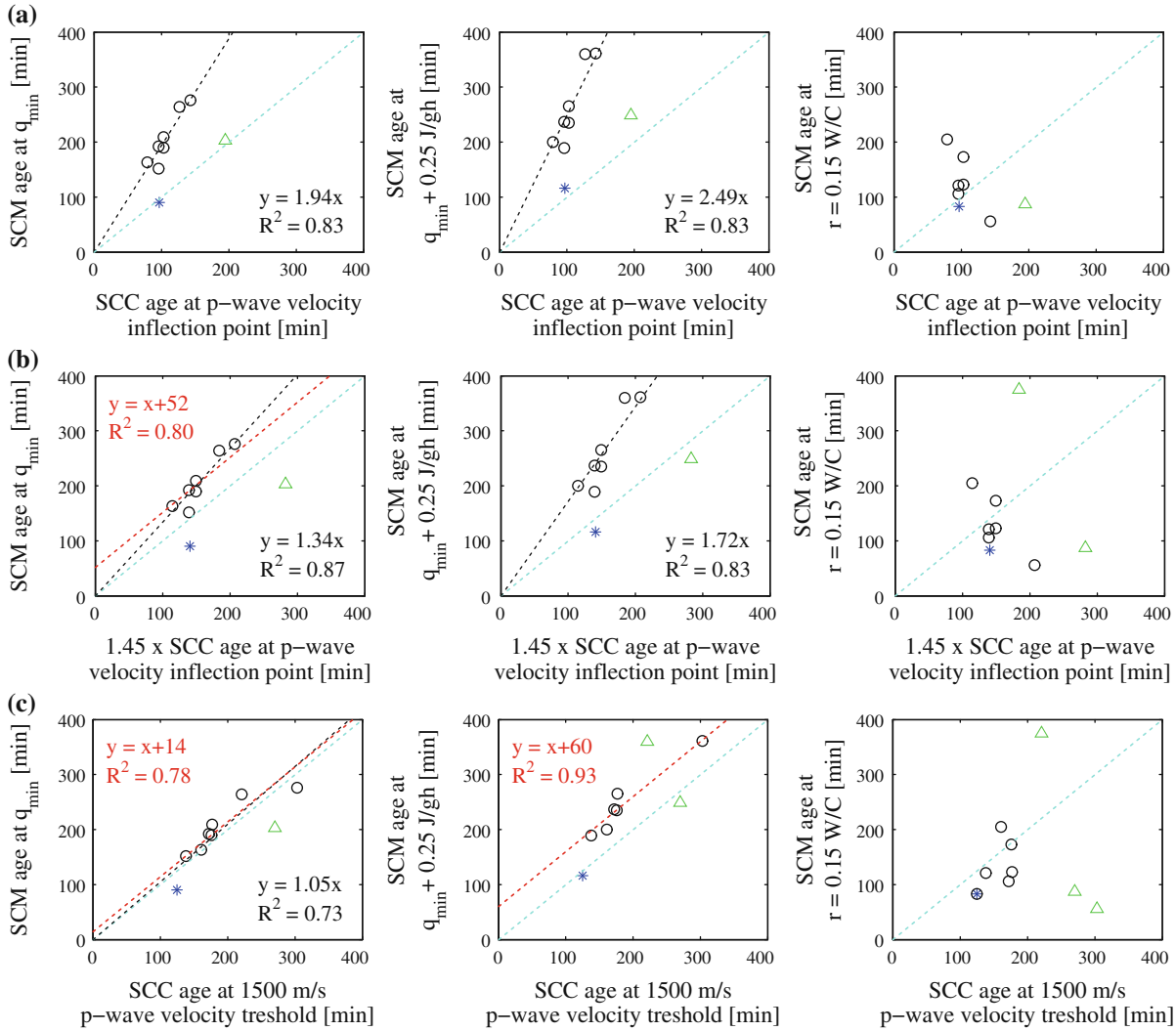

Fig. 10 UT-related key concrete ages ((**a**) age at p-wave velocity curve inflection point, (**b**) 1.45 × age at p-wave velocity curve inflection point, (**c**) age at 1500 m/s p-wave velocity threshold) as a function of isothermal calorimetry related key concrete ages, related to the initial setting. Results used for correlation (*circles*), TC/TM20 result (*star*), outlying results not used for correlation (*triangles*). Correlation lines, equations and R^2 (*black and red dashed lines*) and $y = x$ (*cyan dashed*)

5.2 Correlations with regard to the end of the setting (Fig. 11)

The concrete age at the 2975 m/s p-wave velocity threshold is an excellent indicator for q_{max}, at least for the combinations of CEM I 52.5 R HES and a limestone filler, thus ignoring the outlying results for SCC/SCM22, 23 and 25. The correlation with the start of the setting according to Schindler is less satisfying, but interestingly, the obtained ratio is very close to 1. The same ratio (and R^2) can be obtained for the correlation between the concrete age at 20% of the p-wave velocity gradient and at q_{max}.

Furthermore, Herb [28] showed that a good estimation of the end of the setting according to ASTM C403 can be obtained by plotting the p-wave velocity trace as a function of the reaction degree $r(t)$, obtained by Eq. 3 from a heat of hydration experiment. The part of this relation after the dormant period can easily be replaced by a bilinear system.

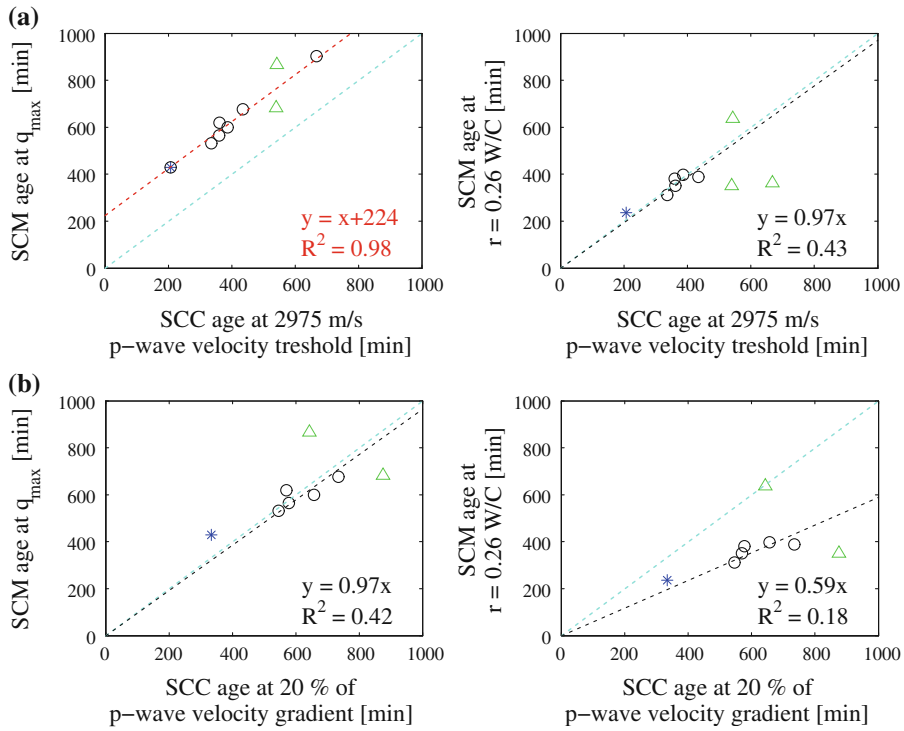

Fig. 11 UT-related key concrete ages ((**a**) age at 2975 m/s p-wave velocity threshold, (**b**) age at 20% of max p-wave velocity gradient) as a function of isothermal calorimetry related key concrete ages, related to the end of the setting. Results used for correlation (*circles*), TC/TM20 result (*star*), outlying results not used for correlation (*triangles*). Correlation lines, equations and R^2 (*black and red dashed lines*) and $y = x$ (*cyan dashed*)

The first, very steep straight line, fitted to the curve up to $r = \pm 0.1$ represents the setting process of the mixture. The second straight line indicates the hardening process of the mixture, and goes from $r = \pm 0.2$ to the r obtained at the end of the shortest of both test. Generally, the ultrasonic test is performed over a considerably shorter period of time than the heat of hydration test. In this case, with the ultrasonic test taking 2 days and the heat of hydration test taking seven days, $r = 0.8$ is obtained. Where both lines cross, the setting period ends and the hardening starts. The reaction degree at this crosspoint is compared to the reaction degree at the end of the setting as proposed by Schindler. Figure 12 shows the ultrasonic p-wave velocity as a function of the reaction degree for SCC/SCM21, with the bilinear approximation according to Herb.

The results are presented in Table 7. A reasonable correspondance is obtained for all SCC/SCM mixtures with an W/C = 0.46.

The argumentation behind Schindler's approach is that the necessary reaction degree to obtain setting,

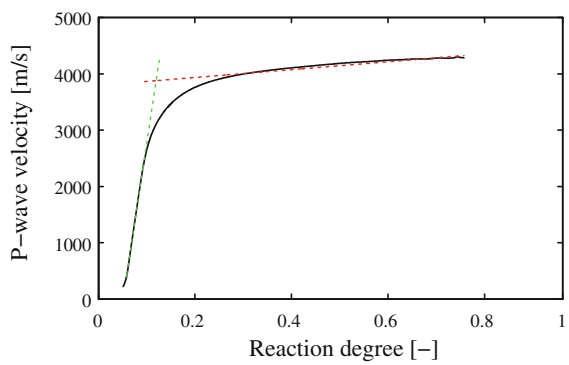

Fig. 12 Ultrasonic p-wave velocity as a function of reaction degree for SCC/SCM21, with bilinear approximation according to Herb [28]

will increase as W/C is raised: The dispersion of the cement grains is higher when more water is present, so that more hydration products are needed to obtain a percolating microstructure. In the case of SCC/SCM however, the dispersion is also determined by the SP.

Table 7 Estimations of the age reaction degree r at the end of the setting, according to Herb [28] and Schindler [35]

Reaction degree r (–) at the end of setting according to	SCC/ SCM20	SCC/ SCM21	SCC/ SCM22	SCC/ SCM23	SCC/ SCM24	SCC/ SCM25	SCC/ SCM26	SCC/ SCM27	TC/ TM20
Herb	0.128	0.124	0.141	0.127	0.112	0.117	0.123	0.120	0.100
Schindler ($r_f = 0.26 \cdot (W/C)$)	0.120	0.120	0.120	0.120	0.120	0.120	0.143	0.143	0.120

Furthermore, the additions that are present in an SCC/SCM mixture become a part of the microstructure. Certainly in the case of limestone additions, when the hydration products precipitate first around these limestone grains, their presence will influence the speed of the formation of this microstructure and might cause the formation of a percolating microstructure at lower reaction degrees. A more specific series of tests might be useful to determine a similar relationship, expanded to take the presence of the SP and the addition into account. The same goes for Schindlers relationship involving the start of the setting.

6 Conclusions

The hydration of a series of self-compacting concretes, one traditionally vibrated concrete and corresponding mortars has been monitored by continuous ultrasonic p-wave velocity and isothermal calorimetry measurements. The compositions differ from each other in the nature and quantity of the addition, the type of superplasticizer and cement, the W/C and C/P ratios. The following conclusions can be made:

- The type of mineral addition has a clear effect on the speed of the formation of the microstructure: Limestone addition accelerates the hydration. This acceleration is more important for a finer limestone powder.
- The influence of the quartz addition on the p-wave velocity and the isothermal heat generation is fairly different, which is also demonstrated in the outlying position of this mixture in the correlation analysis. A more detailed study of the effect of this addition is needed to clarify this ambiguity. For the fly ash there is also a larger difference between some of the ultrasonic and the heat rate parameters, though in general, a small delay and large decelerating effect is observed.
- A polycarboxylate ether extends the time to the start of the setting and slows down the speed of the formation of the microstructure. This delay can however vary significantly from one SP to another. In general, this effect predominates all others, so that all SCC/SCM mixtures are delayed compared to the TC/TM mixture.
- The coarser blast furnace slag cement results in a delay and a deceleration in both tests. The effect on the isothermal hydration rate is much higher, so that it was excluded for a number of the correlation sets.
- The large amount of coinciding parameter variations prevents deducting certain conclusions, since the effects of these parameters tend to amplify, or annihilate each other. This calls for a more detailed parameter study of the different SCC/SCM components used in this research.
- A good correlation is obtained between a number of key concrete ages determined with the ultrasonic and the isothermal calorimetry test. This indicates that the changes in the kinetics of the hydration, caused by the changes in the mixture composition, affect the p-wave velocity and the isothermal heat generation in the same way, but not necessarily in the same amount. The different correlation parameters quantify the relationship between the parameters of both tests. These good correlations demonstrate the meaningfulness of continuous ultrasonic testing in SCC and of the presented p-wave velocity curve parameters when quantifying the influence of the mixture composition on the hydration kinetics.
- Related to the start of the setting, excellent correlations are obtained for the relationship between the start of the setting as determined by Robeyst [15] and the age at which q_{min} is reached and between the age at which the 1500 m/s p-wave velocity threshold is reached and the start of the setting according to Zingg [36].

– Related to the end of the setting, the best correlations are obtained between the age at which the 2975 m/s p-wave velocity threshold is reached and the end of the setting as determined by Schindler, and between the ages at which 20% of the p-wave velocity gradient and q_{max} are reached.

Acknowledgements The authors would like to thank the Research Foundation-Flanders (FWO-Vlaanderen), for their financial support.

References

1. Skarendahl A, Petersson Ö (2000) Self-compacting concrete, state-of-the-art report of RILEM Technical Committee 174-SCC, RILEM Publications s.a.r.l., Cachan
2. De Schutter G, Bartos PJM, Domone P, Gibbs J (2008) Self-compacting concrete. Whittles Publishing, Caithness
3. Etsuo S, Takayuki K, Tomomi S, Kiyoshi A, Masaki D (2006) Influence of superplasticizers on the hydration of cement and the pore structure of hardened cement. Cem Concr Res 36(11):2049–2053
4. Fajun W, Grutzeck M, Roy D (1985) The retarding effects of fly-ash upon the hydration of cement pastes—the first 24 hours. Cem Concr Res 15(1):174–184
5. De Belie N, Grosse CU, Kurz J, Reinhardt HW (2005) Ultrasound monitoring of the influence of different accelerating admixtures and cement types for shotcrete on setting and hardening behaviour. Cem Concr Res 35(11): 2087–2094
6. Lothenbach B, Le Saout G, Gallucci E, Scrivener K (2008) Influence of limestone on the hydration of Portland cements. Cem Concr Res 38:848–860
7. Poppe AM (2004) Influence of fillers on hydration and properties of self-compacting concete. PhD thesis, Magnel Laboratory for Concrete Research, Ghent University
8. Poppe AM, De Schutter G (2005) Cement hydration in the presence of high filler contents. Cem Concr Res 35: 2290–2299
9. Ye G, Liu X, Poppe AM, De Schutter G, Van Breugel K (2007) Numerical simulation of the hydration process and the development of microstructure of self-compacting cement paste containing limestone as filler. Mater Struct 40:865–875
10. Poppe AM, De Schutter G (2006) Analytical hydration model for filler rich self-compacting concrete. J Adv Concr Technol 4(2):259–266
11. Robeyst N, Gruyaert E, Grosse CU, De Belie N (2008) Monitoring of the setting of concrete containing blast-furnace slag by measuring the ultrasonic p-wave velocity. Cem Concr Res 38:1169–1176
12. Akkaya Y, Voigt T, Subramiam KV, Shah SP (2003) Nondestructive measurement of concrete strength gain by an ultrasonic wave reflection method. Mater Struct 36(8): 507–514
13. Reinhardt HW, Grosse CU (2005) Advanced testing of cement based materials during setting and hardening. Report of RILEM Technical Committee 185-ATC, RILEM Publications s.a.r.l., Bagneux
14. Voigt T, Grosse CU, Sun Z, Shah SP, Reinhardt HW (2005) Comparison of ultrasonic wave transmission and reflection measurements with P- and S-waves on early age mortar and concrete. Mater Struct 38(8):729–738
15. Robeyst N (2009) Monitoring Setting and Microstructure development in fresh concrete with the ultrasonic through-transmission method. PhD thesis, Magnel Laboratory for Concrete Research, Ghent University
16. Grosse CU, Reinhardt HW, Krüger M, Beutel R (2006) Ultrasound through-transmission techniques for quality control of concrete during setting and hardening. In: Proceedings of the advanced testing of fresh cementitious materials, Stuttgart, pp 83–93
17. Kraus M, Hariri K (2006) Determination of initial degree of hydration for improvement of early-age properties of concrete using ultrasonic wave propagation. Cem Concr Compos 28(4):299–306
18. Sayers C, Grenfell R (1993) Ultrasonic propagation through hydrating cements. Ultrasonics 31(3):147–153
19. Trtnik G, Turk G, Kavcic F, Bosiljkov VB (2008) Possibilities of using the ultrasonic wave transmission method to estimate initial setting time of cement paste. Cem Concr Res 38(11):1336–1342
20. Van Den Abeele K, Desadeleer W, De Schutter G, Wevers M (2009) Active and passive monitoring of the early drying process in concrete using linear and nonlinear acoustics. Cem Concr Res 39(5):426–432
21. De Schutter G, Desadeleer W, Van Den Abeele K, Wevers M (2006) Degree of hydration based analysis of online monitoring of hardening concrete using acoustic emission (AE) and nonlinear elastic wave spectroscopy (NEWS). In: Proceedings of the advanced testing of fresh cementitious materials, Stuttgart, pp 147–156
22. Lee H, Lee KM, Kim YH et al (2004) Ultrasonic in-situ monitoring of setting process of high-performance concrete. Cem Concr Res 34(4):631–640
23. Harker AH, Temple JAH (1988) Velocity and attenuation of ultrasound in suspensions of particles in fluids. J Phys D Appl Phys 21:1576–1588
24. Biot M (1956) Theory of propagation of elastic waves in a fluid-saturated porous solid. J Acoust Soc Am 28(2): 168–191
25. Bourbié T, Coussy O, Zinszner B (1986) Acoustique des milieux poreux. Publications de l'Institut français du pétrole 27, France
26. Kieffer SW (1977) Sound speed in liquid-gas mixtures: water-air and water-steam. J Geophys Res 82(20):2895–2904
27. Mavko G, Mukerji T, Dvorkin J (2003) The rock physics handbook: tools for seismic analysis of porous media. Cambridge University Press, Cambridge
28. Herb A (2003) Indirekte Beobachtung des Erstarrens und Erhärtens von Zementleim, Mörtel und Beton mittels Schallwellenausbreitung, Universität Stuttgart, Stuttgart
29. Kamada T, Uchida S, Rokugo K (2005) Nondestructive evaluation of setting and hardening of cement paste based on ultrasonic propagation characteristics. J Adv Concr Technol 3(3):343–353

30. Kadri EH, Aggoun S, De Schutter G, Ezziane K (2009) Combined effect of chemical nature and fineness of mineral powders on portland cement hydration. Mater Struct 43(5):665–673
31. Baert G, De Belie N, De Schutter G, Hoste S (2007) Thermal analysis of cement-fly ash pastes. In: Proceedings of the 5th international RILEM symposium on self-compacting concrete, Ghent, pp 583–588
32. Leemann A, Winnefeld F (2007) The effect of viscosity modifying agents on mortar and concrete. Cem Concr Comp 29(5):341–349
33. Lootens D, Jousset P, Martinie L, Roussel N, Flatt RJ (2009) Yield stress during setting of cement pastes from penetration tests. Cem Concr Res 39(5):401–408
34. Nonat A, Mutin JC (1992) From hydration to setting. In: Proceedings of the international RILEM workshop hydration and setting of cements, London, pp 171–191
35. Schindler AK (2004) Prediction of concrete setting. In: Proceedings of the international RILEM symposium on concrete science and engineering: a tribute to Arnon Bentur
36. Zingg A, Winnefeld F, Holzer L, Pakusch J, Becker S, Figi R, Gauckler L (2009) Interaction of polycarboxylate-based superplasticizers with cements containing different C3A amounts. Cem Concr Compos 31(3):153–162
37. Heirman G, Hendrickx R, Vandewalle L, Van Gemert D, Feys D, De Schutter G, Desmet B, Vantomme J (2009) Integration approach of the Couette inverse problem of powder type self-compacting concrete in a wide-gap concentric cylinder rheometer Part II. Influence of mineral additions and chemical admixtures on the shear thickening flow behaviour. Cem Concr Res 39(3):171–181
38. Schindler AK, Folliard KJ (2005) Heat of hydration models for cementitious materials. ACI Mater J 102:24–33
39. Heirman G, Vandewalle L, Van Gemert D (2007) Influence of mineral additions and chemical admixtures on setting and volumetric autogenous shrinkage of SCC-equivalent mortars. In: Proceedings of the 5th international RILEM symposium on self-compacting concrete, Ghent, pp 553–558
40. Heirman G, Vandewalle L, Van Gemert D, Elsen J, Boel V, Audenaert K, De Schutter G, Desmet B, Vantomme J (2007) Influence of mineral additions and chemical admixtures in SCC on microcracking and durability: overview of a belgian research project. In: Proceedings of the 5th international RILEM symposium on self-compacting concrete, Ghent, pp 773–778
41. Heirman G, Vandewalle L, Van Gemert D, Boel V, Audenaert K, De Schutter G, Desmet B, Vantomme J (2008) Time-dependent deformations of limestone powder type self-compacting concrete. Eng Struct 30(10): 2945–2956
42. Steinkamp, Büssenschütt (2007) IP-8 Ultrasonic-Multiplex-Tester instruction manual. Ultratest Gmbh, Bremen
43. De Schutter G, Taerwe L (1995) General hydration model for Portland cement and blast furnace slag cement. Cem Concr Res 25(3):593–604
44. Mills RH (1966) Factors influencing cessation of hydration in water cured cement pastes. Highway Research Board special report 90. Highway Research Board, Washington, pp 406–424
45. Desmet B, Group S, Vantomme J, De Schutter G, Lesage K, Vandewalle L (2010) Parametric study of the effects of the composition on the setting of self-compacting mortar, using continuous ultrasonic monitoring. In: Proceedings of the 6th international RILEM symposium on self-compacting concrete, vol II, Montreal, pp 971–980
46. Bentz DP (2006) Influence of water-to-cement ratio on hydration kinetics: simple models based on spatial considerations. Cem Concr Res 36(2):238–244
47. Pera J, Husson S, Guilhot B (1999) Influence of finely ground limestone on cement hydration. Cem Concr Compos 21(2):99–105
48. Boel V (2006) Microstructuur van zelfverdichtend beton in relatie met gaspermeabiliteit en duurzaamheidsaspecten. PhD thesis (Dutch), Magnel Laboratory for Concrete Research, Ghent University
49. Sahmaran M, Christianto HA, Yaman IO (2006) The effect of chemical admixtures and mineral additives on the properties of self-compacting mortars. Cem Concr Res 28: 432–440
50. De Schutter G, Audenaert K (2007) Durability of self-compacting concrete. State-of-the-Art report of RILEM Technical Committee 205-DSC, RILEM publications s.a.r.l., 2007, Bagneux
51. Henahara S, Yamada K (2008) Rheology and early age properties of cement systems. Cem Concr Res 38(2): 175–195
52. Philippidis TP, Aggelis DG (2005) Experimental study of wave dispersion and attenuation in concrete. Ultrasonics 43:584–595
53. CBR Cementbedrijven, Afdeling Technische Voorlichting (2006) Portlandcement CEM I. Technical data file, Brussels
54. Langan BW, Weng K, WArd MA (2002) Effect of silica fume and fly ash on heat of hydration of Portland cement. Cem Concr Res 32(7):1045–1051
55. Zhou J, Ye G, Van Breugel K (2006) Hydration of Portland cement blended with blast furnace slag at early age, 2nd international symposium on advances in concrete through science and engineering, Quebec (CD-ROM)